

# Spatial Phase Synchronisation of Pistachio Alternate Bearing

Kenshi Sakai (✉ [ken@cc.tuat.ac.jp](mailto:ken@cc.tuat.ac.jp))

Tokyo University of Agriculture and Technology

Patrick Brown

University of California, Davis

Todd Rosenstock

World Agroforestry

Shrini Upadhyaya

University of California, Davis

Alan Hastings

University of California, Davis

---

## Research Article

### Keywords:

**Posted Date:** February 22nd, 2022

**DOI:** <https://doi.org/10.21203/rs.3.rs-877774/v2>

**License:**   This work is licensed under a Creative Commons Attribution 4.0 International License.

[Read Full License](#)

---

# Abstract

Collective dynamics of chaotic oscillators has attracted much attention in many fields even including agriculture and forestry. Alternate bearing of tree crops is a phenomenon in which a year of heavy yield is followed by a light yield. This phenomenon has been modelled using a tent map known as a resource budget model (RBM). We applied in-phase/out-of-phase analysis to yield data of a 9,562 pistachio plants population and revealed phase transitions and mode locking in the orchard. Using a developed network model consisting of diffusively coupled chaotic oscillators (RBMs) on which common noise imposed, we theoretically confirm the phase transitions mode locking and 1/3 power-law scaling in the yield data. Here, we demonstrate how three essential factors, i.e. common noise, direct coupling, and cropping coefficient gradient, explain the spatial synchrony of the orchard.

## Introduction

Alternate bearing (biennial bearing) is a common synchronisation in several tree crops in which a year of heavy yield (on-year state) is followed by a light yield (off-year state). Citrus (e.g. oranges, lemons, and mandarins) and nuts (e.g. pistachio, pecan, and walnuts) are typical alternate bearing crops<sup>1-9</sup> that generally show dominant period-two cycle synchronisation. Masting is also a prevalent synchronisation among tree species in which there are multiple and mixed cycles (i.e. period-two, period-three, period-four, or a combination of them)<sup>10-14</sup>. Such a large on-off period-two cycle of crop production negatively affects profitability and resource (water, nutrient, labor) efficiency. To obtain the knowledge to suppress or predict alternate bearing, the strength of the spatial synchrony should be measured in both individual trees and a population. As the conventional index of synchronisation  $SYNC = \frac{S_{by}}{S_{wy}S_{by}}$  ( $S_{by}$ : standard deviation of between years,  $S_{wy}$ : within years standard deviation) is based on “amplitude” synchronisation, the index determines the degree of synchrony only for a given population<sup>12-14</sup>. Instead, by focusing on “phase” synchronisation, Prasad et al. (2017) and Sakai et al. (2019) developed an in-phase/out-of-phase analysis technique<sup>15</sup> to determine the strength of the phase synchrony both in individual and population levels for Citrus and *Zerkova seratta*<sup>16</sup>. The yield data that were analysed here are remarkable since they included measurements pertaining to 9,562 trees obtained over six years<sup>17</sup>. In this study, by introducing the in-phase/out-of-phase analysis technique, we successfully determined the strength of the phase synchronisation in individual trees and uncovered unique and important features of spatial synchrony in the orchard, i.e. a west-east running gradient of the strength of the in-phase synchronisation, and the phase transition between “order” (in-phase synchronisation) and “disorder” over spatial and temporal (year) domains. Additionally, we demonstrated the spatial distribution of the fraction of the period-two cycle for each tree and each year.

A resource budget model (RBM), which is a tent map<sup>18</sup>, has been previously used to model the dynamics of seed production of perennial plant species<sup>7-9, 12-17</sup>. For cross-pollinating species, the global coupled map (GCM) and local coupled map (LCM) of RBMs have been used with mean-field pollen coupling to

establish the pollen limitation theory as an endogenous mechanism<sup>12-14, 18-20</sup>. Conversely, the pollen limitation theory cannot be observed for deciduous species such as pistachio, as male trees supply pollen to female trees and pollen coupling between female trees never occurs. Instead, the concept of common noise-induced synchronisation (CNIS) was introduced to explain the alternate bearing of pistachio trees<sup>7-9, 21</sup>. These models are all prevalent in nonlinear physics<sup>22-26</sup>. Common noise synchronization is a phenomenon in which a nonlinear (even chaotic) oscillator population is synchronized when an irregularly fluctuating external force acts identically on all the oscillators.

A long-range spatial correlation with 1/3 scaling of spatial correlation was observed. We hypothesised the presence of the direct coupling premising underground root grafting/mycorrhizal networks<sup>1, 27-34</sup> based on the Ising model<sup>17, 18, 21, 35-36</sup>. In this study, we implement a diffusive coupling that enhances the in-phase synchronisation.

By applying the in-phase/out-of-phase technique on both the yield data of the orchard and the numerical experiments, we concluded that common noise, local direct coupling, and the spatial gradient of the cropping coefficient (the control parameter of the RBM) were essential factors that explain unique features i.e., a west-east running gradient of the strength of the in-phase synchronisation, the phase transition and mode locking in the orchard.

## Results

### Spatial phase synchronisation identified in the orchard

Figure 1. Spatial distributions of the in-phase synchronisation in the orchard.

To explain the spatial synchrony of the orchard, the indices for phase synchronisations were defined as described in the Method-Statistics section. Figure 1(a) displays the spatially distributed fraction of the in-phase ( $f_{in}^i(t)$ ) for 9,562 individual trees from 2002–2007. To conduct this analysis the orchard was divided into fourteen blocks by rows and columns: (row, column) = (2 × 7).  $f_{in}^i$  were calculated for each tree  $i$  within the block to which tree  $i$  belonged to.  $f_{in}^i$  was high enough to reach 1.0 in the west blocks and was as low as 0.7 in the east blocks. Figure 1(c) shows  $F_{IN}^K$  ( $K = 1, 2, \dots, 30$ ), which is the average  $f_{in}^i$  for every five columns.  $F_{IN}^L$  ( $L = 1, 2, \dots, 8$ ) is the south to north directional average of  $f_{in}^i$  for every eight rows.  $F_{IN}^K$  drops from 0.92 to 0.7 from west to east (Fig. 2(b)). Conversely, only a small gradient of  $F_{IN}^L$  was observed along the south-north direction (Fig. 2(c)). These results indicate that the strength of the phase synchronisation significantly decreases from west to east but is trivial in the south-north direction. In other words, a significant phase transition is observed from order to disorder in the west-east direction since perfect synchronisation (order) and desynchronization (disorder) of a population corresponds to  $F_{IN}$  to 1.0 and 0.5 respectively. We applied  $I(d)$ , which is known as Moran's I, as the index for the spatial

correlation<sup>29-31</sup> as shown in Fig. 1(d). The six years averaged  $\ell(d)$  of the yield data exhibit a 1/3 power-law scaling as plotted in red.

Figure 2 shows the time evolution of the spatial distribution of phase synchronization in the five periods of two successive years: [2002-2003], [2003-2004],[2004-2005],[2005-2006] and [2006-2007] in five rows, respectively. The first and second columns represent the spatial distributions of  $f_{in}^i$  and  $F_{IN}^K(t)$  vs.  $K$  plot. In the first period [2002-2003], the strength of phase synchronization and spatial distribution of phase synchronization were weak compared to other periods, which is shown in Fig. 2(a) and Fig. 2(f).

In the second to the third periods;[2003-2004] and [2004-2005], the strength of phase synchronization increased, and the spatial distribution of phase synchronization from west to east became distinct, that is, it was stronger in the west and weaker in the east. In fact,  $F_{IN}^1(2004)$  and  $F_{IN}^{30}(2004)$  were 0.98 and 0.56, indicating perfect phase synchronization and desynchronization, respectively. For the fourth [2005-2006] and fifth [2006-2007] periods, the perfect phase synchronisations dominate; thus,  $f_{in}^i(2006)$  and  $f_{in}^i(2007)$  reach 1.0 over the entire orchard, and  $F_{IN}^K(2005)$  and  $F_{IN}^K(2006)$  values are almost always 1.0 for the whole orchard ( i.e.,  $K=1,2,...,30$ ). It is very important that the perfect synchronization mode lasted for two periods [2005-2006] and [2006-2007]. This is clear experimental evidence that mode-locking can occur in a real orchard.

Figures 1 and 2 show that the phase transition between “order” and “disorder” emerge both spatially and temporally (annually) in the orchard. As described above, the index of the fractions of the in-phase such as  $f_{in}^i(t)$ ,  $f_{in}^i$ ,  $F_{IN}^K(t)$  and  $F_{IN}^K$  successfully describe detailed information on how the features of phase synchronisations behave both spatially and temporally.

## The states of “on-year” and “off-year”

In this section, we identify the states of the “on-year” and “off-year” of a population by introducing the phase synchronisation analysis technique (see METHODS section). The phase angle  $\theta_i(t)$  of each tree for each year calculated from eq.(7) determined the “on” and “off” states for the individual trees. The states of “on-year” and “off-year” are defined by the period of time covered as follows; an on-year is one in which the phase angle  $\theta$  is positive, or the yield  $x(t)$  is greater than the average yield of the period  $\bar{x}(t)$  and vice versa<sup>16</sup>.

$$\text{on-year: } \cos\theta > 0 \text{ or } x(t) > \bar{x}(t)$$

$$\text{off-year: } \cos\theta \leq 0 \text{ or } x(t) \leq \bar{x}(t)$$

1

The vector point for each subpopulation block is given by the mean of all coordinates of the dots i.e. ( $\frac{1}{n} \sum_{i=1}^n \cos\theta_i(t)$ ,  $\frac{1}{n} \sum_{i=1}^n \sin\theta_i(t)$ ), where  $n$  is the subpopulation size. The amplitude of the vector is the

order parameter  $p(t)$  of the subpopulation.

$$p(t) = \sqrt{\left(\frac{1}{n} \sum_{i=1}^n \cos \theta_i(t)\right)^2 + \left(\frac{1}{n} \sum_{i=1}^n \sin \theta_i(t)\right)^2}.$$

2

Values  $p = 1$  and  $0$  represent perfect phase synchronisation and desynchronisation, respectively. The “on-year” and “off-year” states of the population are distinguished by the red and black arrows. For example, in 2002 and 2007, all seven blocks are “on-year” states and the states are identical between the seven sub-populations and the whole population. However, in 2003, the state of each subpopulation shifted from a weak “on-year” state to “off-year” states in west to east. The coexistence of the “on-year” and “off-year” states within pistachio orchards has only been known as general qualitative knowledge. With this novel technique, we can quantitatively visualise the coexistence of the “on-year” and “off-year” states of individual trees in both spatial and temporal (annual) domains.

Figure 4 shows the composition of periods in individual trees and the population. Several researchers have reported that alternate bearing of pistachios do not always exhibit a clear two-year cycle but may feature various types of synchronisations both spatially and annually<sup>20,36–38</sup>. Sakai et al. (2019) proposed a practical approach to determine the composition of periodic components of alternate bearing and masting of plant populations<sup>16</sup>. For instance, period-two and period-three sequences are defined as ‘ON ⇒ OFF ⇒ ON’ and ‘ON ⇒ OFF ⇒ OFF ⇒ ON’, respectively (see METHODS-*Fraction of period* section). We mathematically determined the states of On and Off in each year for individual trees with  $ON_i(t)$  and the spatial distributions of  $ON_i(t)$  for 6 years are displayed in Fig. 4-(a)-(f). Wild tree spaces, generally have a wide-ranged spectrum of periods in which variable periods such as period-two, period-three, period-four, and more, including aperiodic motions, exist. For example, period-three was dominant for *Zerkova serrata* but period-four and period-five were non-trivial<sup>16</sup>. For tree crops, their synchronisations occurred generally on a two-year cycle (i.e. period-two), which is why “alternate” bearing and/or “biennial” bearing has become common terminology in pomology<sup>1</sup>. Using the fractions of periods  $FR(Q)$  (see METHODS-*Fraction of period* section), we successfully display the spatial distributions of the compositions of period-two, period-three, period-four and period-five for individual trees of the orchard in Fig. 4 (g)-(j). Figure 4 (g)-(j) indicate the fractions of period-two, period-three, period-four and period-five, which are  $FR(2) = 0.517$ ,  $FR(3) = 0.103$ ,  $FR(4)=0.0244$  and  $FR(5)=0.0060$ , respectively. Obviously, “period-two” is dominant in the orchard. However, from a farm management point of view, it is informative to identify those trees whose cycles are three years, four years or five-years. For example, in the eastern area, the fraction of period-two  $FR(2)$  is smaller than that in the west; further, the fraction of period-three  $FR(3)$  in the east is larger than that in the west. For another example, from the 9,562 trees, we can identify 57 trees whose period are five-years and investigate why they behave in this unique manner.

The results from the novel approach applied to the yield data of the orchard uncover unique and important features of the phase synchronisations in the orchards:

- (1) The gradient of the strength of in-phase synchronisation from west to east.
- (2) The phase transition from order (perfect in-phase synchronisation) to disorder (desynchronisation).
- (3) The occurrence of perfect synchronisation in the whole orchard (mode locking).

To infer from these findings and explain the observed phase synchronisation, we developed a model. The structure of the model was a network of oscillators, which were the RBMs for all the trees; a common noise (external force)  $e_C(t)$  was identically imposed on all the trees in each year  $t$ . We employed diffusive coupling as the direct coupling of the network and considered the coupling timing in the growth stage of a plant. The detail of the model is given in the METHODS- *model development section*)

## Essential factors in the spatial synchronisation of the orchard

Figure 5 shows that the common noise, local coupling, and gradient of the cropping coefficient are essential factors. Given the combinations of the essential parameters ( $\varepsilon, e_C, \alpha, \beta$ ), the best fit common noise (external force)  $e_C(t)$  and initial values of  $S_i(1)$  ( $i = 1, 2, \dots, 9,562$ ) for 25-year periods are determined as follows. The random initial values of  $S_i(1)$  for 9,562 trees are given by homogenous random number in  $(L_T - P_0, L_T)$ . The model runs until  $t$  becomes 500 and the best fit 25 years period in terms of  $F_{IN}^K$  ( $K=1,2,\dots,30$ ) is subsequently selected. The spatial correlation  $l(d)$  diagrams and the spatial distribution of  $\dot{I}_{in}^i$  maps are exhibited in the left column and the right column, respectively.

According to the above three findings, the results, and previous work, we assume that the common noise (external environmental force) ( $e_C$ ), gradient of cropping coefficient ( $m$ ), and direct coupling ( $\varepsilon$ ) are the three essential factors in the model. The range of coupling is set  $r=13$  m so that one tree coupled with neighbouring twelve trees at most. Three characteristics of the spatial correlation are observed in the orchard: (i) high short-range spatial correlation, (ii) long-range spatial correlation with 1/3 power-law scaling, and (iii) wide range variation of  $l(d)$  on the time (year) domain.

In this section, we validate the effects of the three parameters on phase synchronisation by considering the characteristics of the spatial correlation.

Numerical experiments with the developed model were conducted to investigate the effect of the essential factors in terms of  $l(d)$ . Here, we use  $l(d)$ , known as Moran's I, as the index of the spatial correlation<sup>39</sup>, the map of  $\dot{I}_{in}^i$  and  $F_{IN}^K$  to compare with the real data shown in Fig. 1-(d),(b) and (a), respectively. Four different values of the set  $(\varepsilon, e_C, \alpha, \beta)$  were tested (Fig. 5).  $m$  and  $\varepsilon$  are the control parameters of the network model and  $e_C$  is the common noise (environmental external force) that generates the phase synchronisation.  $\alpha$  and  $\beta$  are the spatial gradients of  $m$  in west-east and south-north directions, respectively. Based on a preliminary parameter study (see S-1), we estimated the values for the essential factors as  $e_C = 0.2$ ,  $\varepsilon = 0.1$  and  $m = R_0 + \alpha x/L_{WE} + \beta y/L_{WE}$  ( $R_0 = 1.1$ ,  $\alpha = 0.6$  and  $\beta = -0.1$ ) i.e.  $(\varepsilon, e_C, \alpha, \beta) = (0.1, 0.2, 0.6, -0.1)$  for Fig. 5(a)-(c). In this case, the spatial correlations ( $l(d)$ ) of the

model satisfies the three characteristics of the orchard as follows; (i) for short-range spatial correlation,  $l(d)$  is up to 0.64 at  $d = 5.2$  m, (ii) for long-range spatial correlation,  $l(d)$  is larger than 0.37 even at  $d = 100$  m with 1/3 power row scaling, and (iii)  $l(d)$  fluctuates widely over the same range as actual data (Fig. 1-(d)). The map of  $f_{in}^i$  (Fig. 5(b)) shows good agreement with that of the real data shown in Fig. 1-(a), and the actual and model plots of  $F_{IN}^K$  plots (Fig. 5(c)) also shows good agreement. In the absence of coupling (second row), the short range spatial correlation (Fig. 5(d)) is much smaller than that of the presence of coupling case (Fig. 5(a)), while the map of  $f_{in}^i$  (Fig. 5(e)) and the actual and model of  $F_{IN}^K$  plots (Fig. 5(f)) show some agreement with the real data in the western area, but not the eastern area. Without common noise case (third row), in Fig. 5(g), the short-range correlation is as high as 0.3 because of the local direct coupling ( $\varepsilon = 0.1$ ). However, all the  $l(d)$ s rapidly drop to zero when  $d = 20$  m, and there is no long-range spatial correlation, no power row scaling, and no yearly fluctuation in  $l(d)$ . The map of  $f_{in}^i$  and the actual and model of  $F_{IN}^K$  plots indicate that there is no significant phase synchronization over the entire orchard (Fig. 5(h) and (i)). These results suggest that common noise is indispensable as an external force and the synchronization observed in the orchard (Fig. 5) should be a type of common noise induce synchronisation.

As the cropping efficiency gradient is given by  $m = R_0 + \alpha x/L_{WE} + \beta y/L_{SN}$ , the absence of  $m$ -gradient is implemented by setting  $\alpha = \beta = 0$ , therefore,  $m$  is 1.1 over the orchard. In this case of without the spatial gradient of the cropping efficiency (Fig. 5(j)), very strong short-range spatial correlation,  $l(d) = 0.98$  exists at  $d = 5.2$  m; however, there is no long-range spatial correlation. Figure 5-(k) and (l) exhibits the spatial phase synchronization with  $f_{in}^i = 1$  over the entire orchard and for 25 years. The results of Figs. 5(j)-(l) suggest that even with the presence of both the common noise ( $e_C$ ) and coupling ( $\varepsilon$ ), the gradient of  $m$  is still necessary to explain the features of long-range spatial correlations and spatial distribution of phase synchronisation in the orchard as observed in Fig. 1.

## Numerical interpretation of the experimental results: How endogenous dynamics and exogenous force generate variable types of phase synchronisations

Using the model with the estimated parameters ;  $(\varepsilon, e_C, \alpha, \beta) = (0.1, 0.2, 0.6, -0.1)$  demonstrated in Fig. 5-(a) and (b), Fig. 6 exhibits how endogenous dynamics and exogenous force generate variable types of phase synchronisations. Figure 6-(a) shows the spatial distribution of  $F_{IN}^K(t)$  of the model. The phase transitions between order and disorder in both space and time (annual) domains were the substantial nature of the dynamics and important behaviour in terms of phase synchronisation.

Resource switching and weather cues act together to cause synchronisation such as masting and alternate bearing (Lyles et al. 2009)<sup>7</sup>. The results described in Fig. 6 confirm this knowledge mathematically. The combination of endogenous dynamics and exogenous forces cause the perfect

phase synchronisations. Figure 6(a) displays the  $F_{IN}^K(t)$  for 25 years. An interesting finding of this analysis is that significantly strong phase synchronisations generally occur when the common noise (external force) is high; however, this is not always the case. Furthermore, almost complete desynchronisation occurs even when a significantly large common noise (external force) is present. The perfect phase synchronisations occur when  $t = 12, 13,$  and  $14$  with  $F_{IN}^K(t) \geq 0.997$  (i.e.  $F_{IN}^K(12) = 0.9975, F_{IN}^K(13) = 1.0,$  and  $F_{IN}^K(14) = 1.0$ ). The almost complete desynchronisations occur when  $t = 4$  and  $7$  with  $F_{IN}^K(t) \leq 0.58$ .

Three consecutive perfect in-phase synchronisations occur when  $t = 12, 13,$  and  $14$ ;  $t = 13$  is an “off-year” as the year ( $t=12$ ) is the second largest “on-year” within 25 years; thus, the production ( $C_f(12)$ ) was zero, because the excess of the threshold ( $L_t=100$ ) of the total amount of  $S(t), P_S(t),$  and  $CE(t)$  becomes the flowering cost  $C_f(t)$  which is proportional to the production  $C_a(t)$ . Consequently, the resource remained in the bodies of the tree, meaning that  $S(13)$  nearly obtained the almost maximum value for all trees. Additionally, that year ( $t=13$ ) had the best condition as  $e_c(13)=0.4$  ( $CE(13)=4$ ) within 25 years, which allowed all the trees to change their states into the maximum on-year state with the perfect in-phase synchronisation (in fact  $F_{IN}^K(13) = 1.0$ ). As a result, the smallest amount of resources remained in the bodies of the trees meaning that  $S(14)$  obtained the minimum value within 25 years (see Fig. 6(c) at  $t=14$ ). The external force was not large ( $CE(14)=2$ ) with no excess (i.e.  $C_f(14)=0$ ) for all trees so that the perfect synchronisation ( $F_{IN}^K(13) = 1.0$ ) still remained in “off-year” state. Thus, three consecutive perfect phase synchronisations in other words, this is the mechanism of the three years consecutive perfect phase synchronisations (i.e. three years mode locking)). If  $CE(14)$  is at least greater than 6,  $t=14$  will be a weak “on-year” state with partial desynchronization and this mode lock will terminate.

In the opposite case,  $t=6$  was an “on-year” with a weak synchronisation mode (see Fig. 6(a)),  $t=7$  should be succeeded by “off-year” if  $CE(7)$  was a normal value. However,  $CE(7)$  was large enough (i.e.  $CE(7) = 3.5$  is the second largest within 25 years,) to keep very weak “on-year” and the model turned to the almost complete desynchronization ( $F_{IN}^K(7) = 0.568$ ). It is interesting to note that the simulation results show that such a large external force causes desynchronization instead of synchronization.

Owing to the historically imposed exogenous forces (accumulated footprints of exogenous forces) on the endogenous dynamics, a mode-locking emerged. We note that two types of “in-phase mode-locking” exist, one which occurred in the “off-year” and another which occurred in the “on-year”. The first one occurred at  $t = 12$  and  $14$ , and the second one occurred at  $t = 13$ . Also two types of “desynchronization mode” exist, one which occurred in the “off-year” and another which occurred in the “on-year”, occurred at  $t=4$  and  $t=7$ , respectively. The perfect in-phase synchronisation (order) and perfect desynchronisation (disorder) were the two extremes. Most of the modes of phase synchronisation appeared either in between or were mixtures of both extremes e.g. Fig. 6.(a) at  $t=20$  and  $23$ . The mode of the mixture may be considered as a “chimaera like state”, which was first experimentally captured in optical-coupled map



lattices in nonlinear physics<sup>40</sup>. Here, we detected the “chimera like state” in the field experiments of the orchard in 2004-2005 period as shown in Fig. 2(h).

## Discussions

The population dynamics of chaotic oscillators is a universal phenomenon of interest in several fields. It has been employed to treat and understand the synchronisation phenomenon of perennial plant populations as mathematical spatio-temporal dynamics in nonlinear physics. This synchronisation phenomenon is also of practical importance in food production, forest production, and ecosystem management. In this study, we assumed that the synchronisation of 9,562 pistachio trees was “a common noise induced synchronisation” in chaotic oscillator networks with local diffusion coupling. By proposing the method of detecting the synchronisation intensity at the population level and individual level, we successfully visualised the spatial distribution of the synchronisation with real data and verified the mathematical model.

The gradient of the strength of phase synchrony is a unique feature of the orchard. The results led us to one conclusion: the cropping coefficient ( $m$ ) increases from 1 to 1.6 from the western part to the eastern part of the orchard over a distance of 780 m. The cropping coefficient  $m$  is the product of the cost ratio  $R_C$  and fertility successes  $Z$ .  $R_C$  is the control parameter of the RBM (e.g.  $-R_C$  is the slope at the fix point of the RBM) ; it might be hard to imagine that  $R_C$  changes from 1 to 1.6 in a population of clone plants. The fertility successes  $Z$ , however, are positively relevant to the pollen density. In the pistachio orchard, male trees are evenly located; thus the pollen density is uniform and the soil type is also uniform with a small geographical slope. It is also hard to assume that  $Z$  changes from 1 to 1.6 in the west to east of the orchard. Therefore, the source of the gradient of the cropping coefficient  $m$  remains an open question. In California, the westerlies might be a candidate source, if the westerlies carry a sufficient amount of pollen from west to east, resulting in the pollen density increasing coherently in a west-east direction in the orchard. This hypothesis must to be validated by intensive field survey of pollen drifting due to the westerlies.

This paper hypothesise that the cause of local coupling is underground interaction between trees through root grafting/mycorrhizal networks as direct-coupling<sup>17,27</sup>. It is a key factor that could explain the long-range spatial correlation of the orchard. By setting the appropriate timing of the direct coupling in the growth stage of a plant, the diffusive coupling of RBMs works to enhance the in-phase synchronisation. This model is designed to realise the dynamics derived from the hypothesis. In the numerical experiments of Fig. 4, the best fit range of direct coupling was 13 m. This implies that direct coupling of root grafting had a range of 26 m. Nevertheless, it is necessary to conduct a field survey to confirm this explanation. Beside the direct local coupling hypothesized here, there is another possible hypothesis that local (spatial) variability of pollen density, soil fertility and/or irrigation for in-direct local coupling. This in-direct local coupling hypothesis should be an interesting future work to deepen our understanding agro-ecological systems.

For suppressing the alternate bearing, the strength of the phase synchronisation in the orchard should be reduced. For example, if the spatial gradient of the phase synchronisation occurs because of the pollen density, the number of male trees in the western area can be increased to ease the alternate bearing. For another example, if the direct coupling caused by the natural root grafting and/or mycorrhizal networks enhances the phase synchronisation, breaking the root networks using a subsoiler or pan-breaker can help remediate the alternate bearing. Thus, clarifying the mechanism of the spatial gradient  $m$  is important for farm management.

This is challenging in terms of both nonlinear physics and farming operations. In orchards and forests, the uniformity of individual trees is ensured, and accurate spatial arrangement information can be easily obtained. Therefore, the proposed approach can be applied to tree crops other than pistachio and forest trees. In other words, nonlinear physics is useful in fruit production, tree production, and ecosystem management and is expected to be widely applied to these fields.

## Methods

### Field experiments

In the orchard with  $N = 9,562$  (Fig. 1), the male pistachio trees were evenly spaced ( $26 \text{ m} \times 26 \text{ m}$ ); female trees were located within 14 m of the nearest male tree to receive enough pollen. The data were obtained from a 32.3-ha ( $416 \text{ m} \times 777 \text{ m}$ ) orchard located at  $35^\circ 86' \text{ N}$ ,  $119^\circ 87' \text{ W}$  (Lost Hills, Kings County, California, USA)<sup>7–9</sup>. The trees were spaced 5.2 m and 6.4 m in rows and columns, respectively. In 2007, the trees in the western part of the orchard were removed, so the total area of the orchard was 22.7 ha<sup>17</sup>.

Synchronisation was exhibited in the annual yield, called alternate bearing, for 2002–2007. The data used here is available as a supplementary dataset. The subset data excluding blank and missing data points from the data is available<sup>17</sup>. Pistachio yield data collection in the orchard was carried out in compliance with the relevant institutional, national and international guidelines and legislation.

### In-phase/out-of-phase analysis technique

**Fraction of in-phase/out-of-phase.** The phase synchronisation of a population comprises two classes: in-phase and out-of-phase<sup>15</sup>. Let  $x_i(t)$  be the yield of the  $i^{\text{th}}$  tree in year  $t$ , and  $\varnothing(i, j, t)$  be the phase between the  $i^{\text{th}}$  and  $j^{\text{th}}$  trees,

$$\varnothing(i, j, t) = \{x_i(t + 1) - x_i(t)\}\{x_j(t + 1) - x_j(t)\}. \quad (3)$$

Then, the fraction of the in-phase behaviour of tree  $i$  relative to the remaining trees in the population (size  $N$ ) in year  $t$  is defined as

$$f_{in}^i(t) = \frac{1}{N-1} \sum_{j=1, j \neq i}^N H(\varnothing(i, j, t)); \quad (4)$$

that is,  $f_{IN}^i(t)$  is the ratio of tree  $i^{\text{th}}$  to be in-phase relative to the rest of the  $N-1$  trees in the population. We denote by  $\bar{f}_{IN}^i$  the time average of  $f_{IN}^i(t)$  for tree  $i$ . The fraction with in-phase behaviour  $F_{IN}(t)$  within the population (size  $N$ ) for year  $t$  is calculated from

$$F_{IN}(t) = \frac{1}{N(N-1)} \sum_{i=1}^N \sum_{j=1, j \neq i}^N f_{IN}^{i,j}(t)$$

5

$f_{IN}^i(t)$  and  $F_{IN}(t)$  quantify the strength (rate) of phase synchronisation for the individual tree and population, respectively.

$F_{IN}^K(t)$  ( $K = 1, 2, \dots, 30$ ) is the west-east directional averages of  $f_{in}^i(t)$  for every 5 columns.  $F_{IN}^L(t)$  ( $L = 1, 2, \dots, 9$ ) is the south-north directional averages  $f_{in}^i(t)$  for every 9 rows, respectively.  $F_{IN}^K$  and  $F_{IN}^L$  are the time (year) averages of  $F_{IN}^K(t)$  and  $F_{IN}^L(t)$ , respectively.

Perfect in-phase synchronisation is when  $F_{IN}$  any size of the population and represents "order". In the case of a population whose size is larger enough,  $F_{IN}=0.5$  indicates all trees behaving completely randomly (i.e. perfect out-of-phase synchronisation) and represents "disorder".

**Fraction of period** <sup>16</sup>. A period- $Q$  sequence is defined as the sequence where one 'on-year' at  $t$  is followed by  $Q-1$  'off-years' and an 'on-year' arises at  $t + Q$ . The fraction of period- $Q$  of  $x_i(t)$  is determined by

$$FP_i(Q) = \frac{Q}{(T-1) - \text{mod}(T-1, Q)} \sum_{t=1}^{T-Q} [ON_i(t) ON_i(t+Q) \prod_{j=1}^{Q-1} \{1 - ON_i(t+j)\}]. \quad (6)$$

where,  $ON_i(t) = \begin{cases} 1 & \text{if } x_i(t) > \bar{x}_i \\ 0 & \text{if } x_i(t) \leq \bar{x}_i \end{cases}$ , "on-year", and  $\bar{x}_i = \frac{1}{T} \sum_{t=1}^T x_i(t)$ .

The phase angle  $\theta(t)$  of a single time series  $x(t)$  is given by

$$\theta(t) = \text{angle} \left( \text{HT} \left[ \frac{x(t) - \bar{x}}{\sigma} \right] \right),$$

7

where HT is the Hilbert transform of the true signal  $X(t)$  and  $\bar{x}$  is the time average of  $X(t)$ .

**Moran's I.** Moran's I is the distance measure of the spatial correlation,

$$I = \frac{N}{W} \frac{\sum_{i=1}^N \sum_{k=1}^N w_{ik} (x_i - \bar{x})(x_k - \bar{x})}{\sum_{i=1}^N (x_i - \bar{x})^2},$$

8

where  $N$  denotes the number of spatial units indexed by  $i$  and  $k$ ;  $x_i$  the yield,  $\bar{x}$  the mean of the yield,  $w(i,k)$  a matrix of spatial weights with zeros on the diagonal ( $i = 1, \dots, N$ ;  $w(i, i) = 0$ ); here,  $W$  is the sum over all  $w(i,k)$ .

$$w(i,k) = \begin{cases} 1 & \text{if } |D(i,k) - r| \leq \Delta d \\ 0 & \text{if } |D(i,k) - r| > \Delta d \end{cases}$$

9

where  $D(i,k)$  denotes the distance between tree  $i$  and tree  $k$ .

## Model development

The tent map, global coupled map (GCM), local coupled map (LCM), and coupled map lattices (CML), and common noise induced synchronisation (CNIS) are all fundamental models in nonlinear physics<sup>22-25</sup>. To understand the spatial synchronisations observed in the orchard, we introduce a novel model here. This model combines CML and CNIS by implementing direct coupling RBMs networks with imposing external force on all trees identically. These popular models in nonlinear physics are also useful for explaining the spatio-temporal collective dynamics in ecological systems.

**Networks of plants.** In addition to the oscillator, we also use the RBM, which is a one-dimensional tent map for a single tree for masting and alternate bearing<sup>18</sup>.  $S^i(t)$  represents the amount of resource reserves at the beginning of year  $t$  for tree  $i$ ,  $P_{-S}(t)$  the additional resource (e.g. photosynthetic residue<sup>18</sup> or unspecified substances<sup>41,42</sup>) being accumulated by flowering season in the trunk of a plant, and  $L_t$  the upper limit of the pool in which the resource is reserved in the plant body.

**Direct Coupling.** The common way of diffusive coupling<sup>21</sup> on RBMs generates out-of-phase behaviour<sup>15</sup>. Conversely, here, to enhance the in-phase synchrony, we implement the coupling in a novel form as

$$S^i(t) = S^i(t) + \frac{1}{N-1} \sum_{j \neq i} \epsilon_{j,i} (S^j(t) - S^i(t))$$

10

where  $\epsilon_{j,i}$  is the coupling strength and  $S^i(t)$  is the amount of resource when material exchanges occur. Thus, we assume that material exchanges occur underground before flowering.

The map  $G: \{S^i(t+1) \rightarrow S^i(t+1)\}$  is

$$S^i(t+1) = \begin{cases} S^i(t) + P_{-S}(t) - C_f^i(t) & \text{if } S^i(t) + P_{-S}(t) \leq L_t \\ S^i(t) + P_{-S}(t) & \text{if } S^i(t) + P_{-S}(t) > L_t \end{cases}$$

"on-year"

$$S^i(t+1) = \begin{cases} S^i(t) + P_{-S}(t) & \text{if } S^i(t) + P_{-S}(t) \leq L_t \\ S^i(t) + P_{-S}(t) - C_f^i(t) & \text{if } S^i(t) + P_{-S}(t) > L_t \end{cases}$$

"off-year"

11

in which the cost of flowering  $C_f^i(t)$  and the cost of fruiting are given by

$$C_{f^i}(t) = \left( \begin{array}{c} SA^i \\ P_S \end{array} \right)_{L_t} + \left( \begin{array}{c} SA^i \\ P_S \end{array} \right)_{L_t} > 0 \quad \left( \begin{array}{c} SA^i \\ P_S \end{array} \right)_{L_t} \leq 0$$

12

,  
and,

$$C_a^i(t) = m C_{f^i}(t)$$

13

where  $m$  is the cropping efficiency given by the product of the cost ratio  $R_C$  and fertility successes  $Z$ .

$$m = R_C Z$$

14

We assume  $m$  varies from tree to tree in the orchard,

$$m_i = R_0 + \alpha \frac{x_i}{L_{WE}} + \beta \frac{y_i}{L_{SN}}$$

15

where  $(x_i, y_i)$  are the spatial coordinates of the  $i^{\text{th}}$  tree.  $L_{WE}$ , and  $L_{SN}$  are the distances from the west end to east end and the south end to north end of the orchard, respectively.

**External force (common noise).** Common noise is  $CE(t)$  the external environmental force imposed on all trees identically.  $CE(t)$  is added on, that is,

$$CE(t) = e_C \sigma$$

16

$$P_S(t) = P_0 \left( 1 + CE(t) \right)$$

17

where  $P_0$  denotes the intrinsic annual surplus and  $\sigma$  is the normal distribution  $\text{N}(\mu, \sigma^2)$ . The level of common noise is represented by  $e_C$ .

## Declarations

### Acknowledgements

K.S thanks Prof. Eliezer Goldschmid (emeritus professor of agriculture at the Hebrew University of Jerusalem), Prof. Awadesh Prasad (Department of Physics and Astrophysics, University of Delhi) and Prof. Rajarshi Roy (Institute for Research in Electronics and Applied Physics, University of Maryland) for productive conversations. KS also thanks JSPS Grant-in-Aid Nos. 20K21347, 23380152, and 15KT0112. AH acknowledges NSF DMS – 1840221 NSF DMS – 184022.

### Author Contributions

K.S., P.B., S.U and A.H. conceived the research. P.B. and R.T. designed the field survey and performed measurements and established the data set. K.S. conducted the numerical simulations and the analysis of the results, and prepared the manuscript. All of them participated in discussions and provided intensive suggestions for improving the manuscript.

### **Correspondence to Kenshi Sakai.**

Email: ken@cc.tuat.ac.jp

### **Ethics declarations**

Competing interests

The authors declare no competing interests.

### **Data Availability**

The data are available in the SUPPLEMENTS section.

## **References**

1. Goldschmidt, E. E. Plant grafting: new mechanisms, evolutionary implications. *Front. Plant Sci.* **5**, 2014.00727,2014
2. Sakai, K. *Nonlinear dynamics and chaos in agriculture systems*, (Elsevier Science, Amsterdam, 2001).
3. Prasad, A. & Sakai, K. Understanding the alternate bearing phenomenon: Resource budget model. *Chaos* **25**, 123102–6 (2015).
4. Li, C-Y., Weiss, D. & Goldshmidt, E.E. Girdling Affects Carbohydrate-related Gene Expression in Leaves, Bark and Roots of Alternate-bearing Citrus Trees. *Ann. Bot.* **92**(1), 137–143(2003).
5. Kon, T.M. & Schupp J.R. Apple crop load management with special focus on early thinning strategies: a US perspective. *Hortic. Reviews.* **46**, 255–298 (2019).
6. Khalil, S.K. et al. Foliar ethephon fruit thinning improves nut quality and could manage alternate bearing in pecan. *Pharm. Chem. J.* **3**, 150–156 (2016).
7. Lyles, D., Rosenstock, T. S., Hastings, A. & Brown P. H. The role of large environmental noise in masting: General model and example from pistachio trees. *J. Theor. Biol.* **259**(4), 701–713 (2009).
8. Rosenstock, T. S., Rosa, U.A., Plant, R. E. & Brown P. H. A reevaluation of alternate bearing in pistachio. *Scientia Horticulture* **124**, 149–152 (2010).
9. Rosenstock T. S., Hastings, A., Koenig, W. D., Lyles, D.J. & Brown P. H. Testing Moran' s theorem in an agroecosystem. *Oikos* **120**, 1434–1440 (2011).
10. Koenig, W. D. & Knopes, J. M. H. The mystery of masting in trees. *American Scientist* **93**, 340–347 (2005).

11. Kelly, D. & Sork, V. L. Mast seeding in perennial plants: why, how, where? *Annu. Rev. Ecol. Syst.* **33**, 427–447 (2002).
12. Satake A. & Iwasa, Y. Pollen Coupling of Forest Trees: Forming Synchronized and Periodic Reproduction out of Chaos. *J. Theor. Biol.* **203**,63–84 (2000).
13. Satake A. & Iwasa, Y. The synchronized and intermittent reproduction of forest trees is mediated by the Moran effect, only in association with pollen coupling. *J. Ecology* **90**, 830–838 (2002).
14. Satake A, & Iwasa Y. Spatially limited pollen exchange and a long-range synchronisation of trees. *Ecology* **83**, 993–1005 (2002).
15. Prasad,A., Sakai,K,. & Hoshino,Y. Direct coupling: a possible strategy to control fruit production in alternate bearing. *Sci. Rep.* **7**, 39890 (2017)
16. Sakai, K., Hoshino, Y., Prasad, A., Fukamachi, A. & Ishibashi, A. Period-3 dominant phase synchronisation of *Zelkova serrata*: n order-collision bifurcation observed in a plant population. *Sci. Rep.* **9**,15568 (2019)
17. Noble A.E., Rosenstock, T. S., Brown, P.B., Machta, J. & Hastings, A. Spatial patterns of tree yield explained by endogenous forces through a correspondence between the Ising model and ecology. *PNAS.***115** (8),1825–1830 (2018)
18. Isagi, Y., Sugimura, K., Sumida, A. & Ito, H. How does masting happen and synchronize? *J. Theor. Biol.* **187**, 231–239 (1997).
19. Akita, T., Sakai, K., Iwabuchi, Y., Hoshino, Y., & Ye, X. Spatial autocorrelation in masting phenomena of *Quercus serrata* detected by multi-spectral imaging. *Ecol Model* **215**(1-3), 217–224 (2008).
20. Crone, E.E. & Rap,J.M. Resource depletion, pollen coupling, and the ecology of mast seeding. *Ann. N.Y. Acad. Sci.* **1322**, 21–34 (2014).
21. Noble A.E., Machta, J.& Hastings, A. Emergent long-range synchronisation of oscillating ecological populations without external forcing described by Ising universality. *Nat Commun.* **6**, 6664 (2015).
22. Kaeko, K. Spatiotemporal Intermittency in Coupled Map Lattices, *Prog. Theor. Physics.* **74**(5), 1033–4044 (1985).
23. Kaneko, K. Globally Coupled Chaos Violates the Law of Large Numbers but Not the Central-Limit Theorem. *Phys. Rev. Lett.* **65**,1391–1394 (1990).
24. Zhou, C. & Kurths, J. Noise-Induced Phase Synchronisation and Synchronisation Transitions in Chaotic Oscillators. *Phys. Rev. Lett.* **88**, 230602 (2002).
25. Pecora, L. M. & Carroll, T. L. Synchronisation in chaotic systems. *Phys. Rev. Lett.* **64**, 821–824 (1990).
26. Rosenblum, M.G., Pikovsky, A.S. & Kurths, J. Phase Synchronization of Chaotic Oscillators. *Phys. Rev. Lett.* **76**(11), 1804–1807(1996)
27. Klein, T., Siegwolf, R. T. W. & Körner, C. Belowground carbon trade among tall trees in a temperate forest. *Science* **352**(6283), 342–344 (2016)
28. Graham, B. & Bormann, F. Natural root grafts. *Bot. Rev.* **32**,255–292 (1966).
29. Lev-Yadun,S. Why should trees have natural root grafts? *Tree Physiol.* **31**,575–578 (2011).

30. van der Heijden, M. G. A. et al. Mycorrhizal fungal diversity determines plant biodiversity, ecosystem variability and productivity. *Nature* **396**, 69–72 (1998)
31. Simard, S. W. et al. Net transfer of carbon between ectomycorrhizal tree species in the field. *Nature* **388**, 579–582 (1997)
32. Gaion, L.A. & Carvalho, R.F. Long-Distance Signaling: What Grafting has Revealed?. *J. Plant Growth Regul.* **37**, 694–704 (2018).
33. Esmaeili, S., Hastings, A., Abbott, K., Machta, J. & Nareddy, V.R. Density dependent Resource Budget Model for alternate bearing. *J. Theor. Biol.* **509**.110498 (2020)
34. Ye, X. & Sakai, K. Limited and time-delayed internal resource allocation generates oscillations and chaos in the dynamics of citrus crops. *Chaos* **23**, 043124 (2013).
35. Ye, X. & Sakai, K. A new modified resource budget model for nonlinear dynamics in citrus production. *Chaos, Solitons and Fractals*. 87.51–60. (2016).
36. Smith, M. W. et al. Long-term performance of 'Ellendale' mandarin on seven commercial rootstocks in sub-tropical Australia, *Sci Hort.* **102**(1), 75–89 (2004).
37. Ferguson, L., Beede, R.H., Reyes, H. & Metheney, P. California Pistachio rootstocks evaluations. *Acta Hort.* **591**, 63–66 (2002).
38. Johnson, R.S. & Weinbaum, S.A. Variation in tree size, cropping efficiency, and alternate bearing among Kerman pistachio trees. *J. Am. Soc. Hortic. Sci.* **112**, 942–945. (1987).
39. Moran P.A.P. The statistical analysis of the Canadian Lynx cycle. 2. Synchronisation and meteorology. *Aust. J. Zool.* **1**, 291–298 (1953).
40. Hagerstorm, A. M., et al. Experimental observation of chimeras in coupled-map lattices. *Nat. Phys.* **8**, 658–661 (2012).
41. Hoch, G., Siegwolf, Rolf T.W., Keel, S. G. Körner, C. & Han, Q. Fruit production in three masting tree species does not rely on stored carbon reserves, *Oecologia* **171**, 653–662 (2013).
42. Tomoaki, I. et al. Are stored carbohydrates necessary for seed production in temperate deciduous trees? *J. Ecol.* **101**, 525–531 (2013).

## Figures



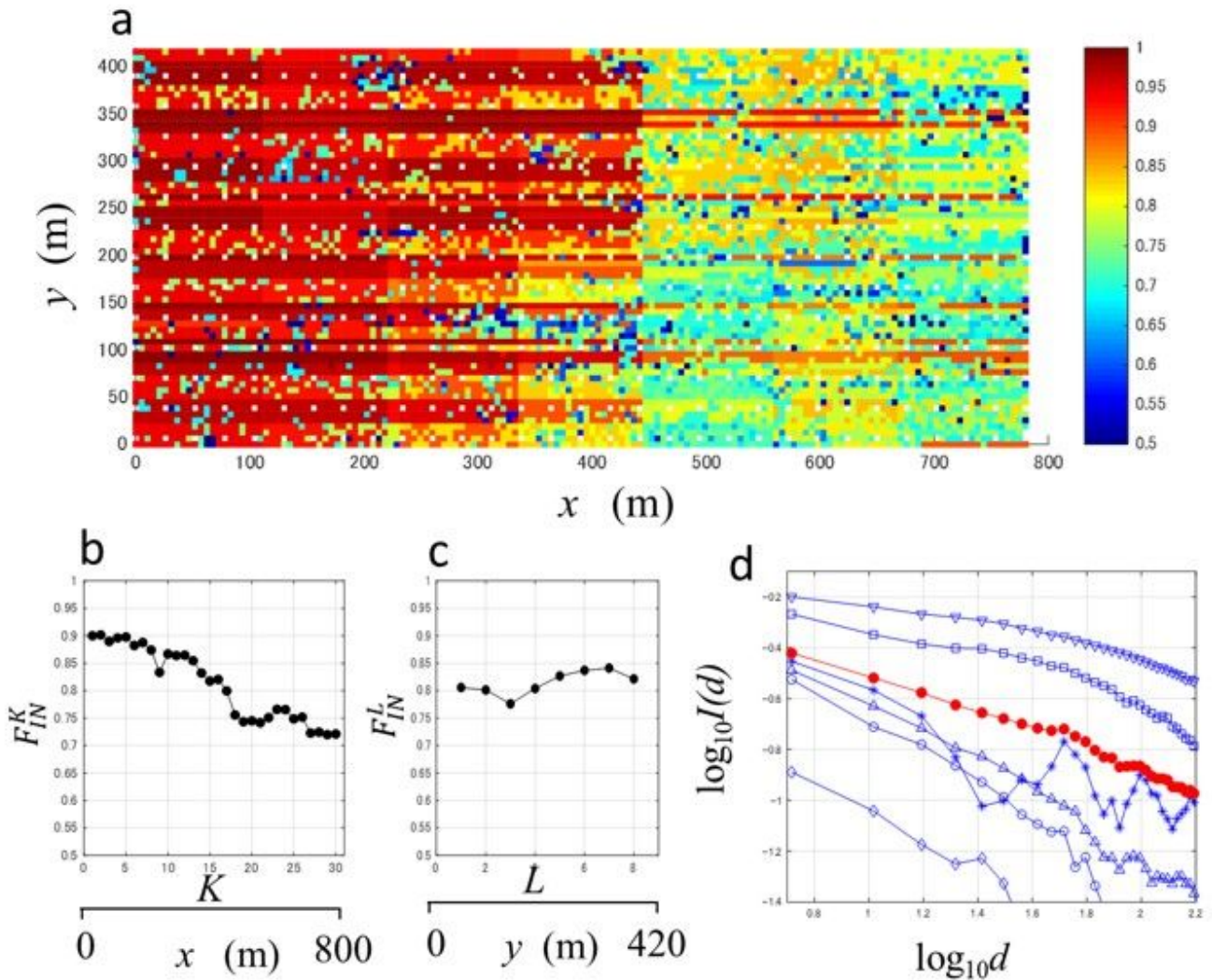


Figure 1. Spatial distributions of the in-phase synchronisation in the orchard.

(a) The actual  $f_{IN}^i$  map for 2002–2007 in eight blocks (7 West-East  $\times$  2 South-North);

(b) Averaged West-East gradient of  $F_{IN}^k$  for 2002–2007; (c) Averaged South-North

gradient of  $F_{IN}^L$  for 2002–2007; (d) time (year) evolution of  $F_{IN}(t)$ .

(d) log-log plot of Moran's I ; I(d) for 6 years below:

\* 2002  $\triangle$  2003  $\nabla$  2004  $\square$  2005  $\diamond$  2006  $\circ$  2007,  $\bullet$  Average

Figure 1

See image above for figure legend.

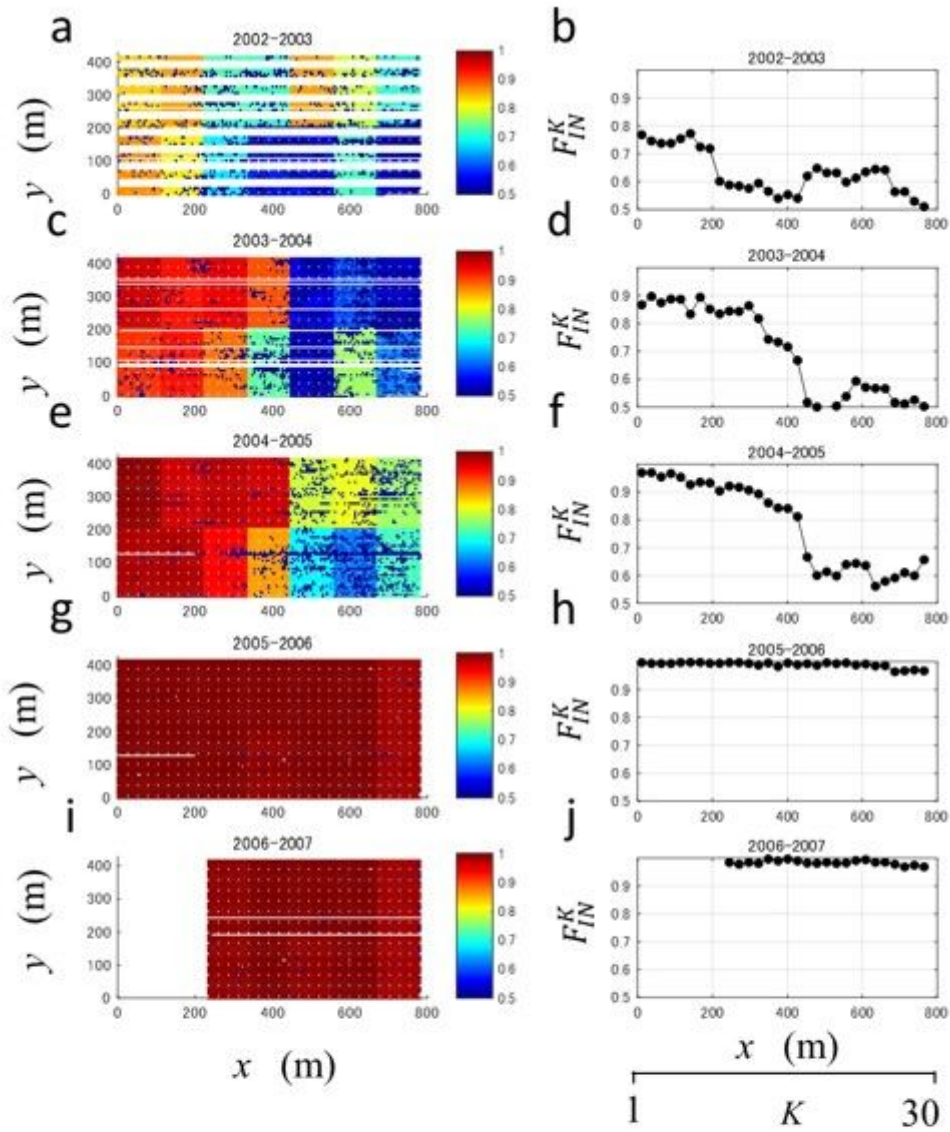


Figure 2. Time evolution of the spatial phase transition of the phase synchronisation (a)-(e) The time (year) changes of the spatial phase synchronisation:  $f_{IN}^i(t)$  maps for 2002–2003, 2003–2004, 2004–2005, 2005–2006, and 2006–2007 periods in the orchard. (f)-(j) The gradient of the strength of the phase synchronisation:  $F_{IN}^K(t)$  vs.  $K$  plots for 2002–2003, 2003–2004, 2004–2005, 2005–2006, and 2006–2007 periods in the orchard

## Figure 2

See image above for figure legend.

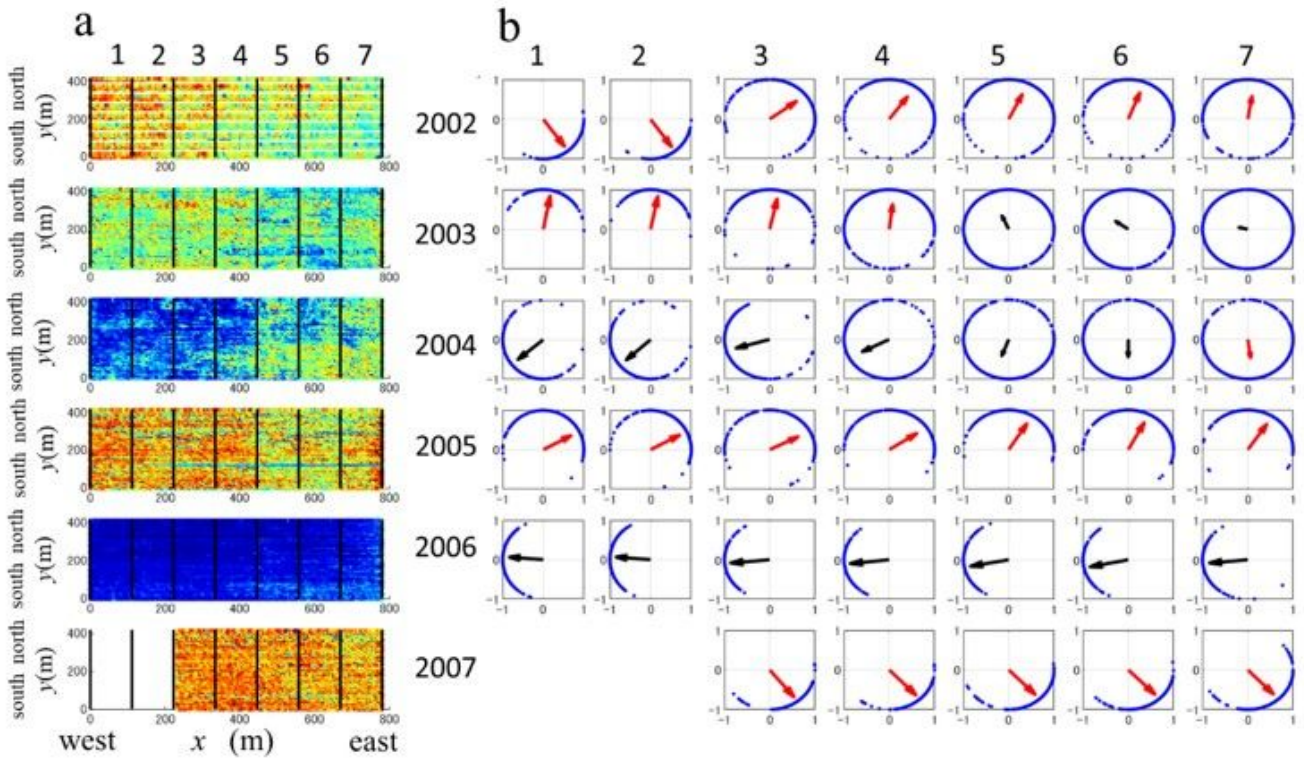


Figure 3 Spatial and annual phase transitions of the states of “on-year” and “off-year” for individual trees expressed by circle maps.

(a) Yield maps for 2002 through to 2007.

(b) Circle maps for the fourteen blocks for six years [2002–2007]. The blue dot mark ( $\cos \theta_i, \sin \theta_i$ ) on the circumference represents the state of tree  $i$ . The vectors represent the on-off state of sub-populations of each block and on and off correspond to the red and black ink, respectively.

### Figure 3

See image above for figure legend.

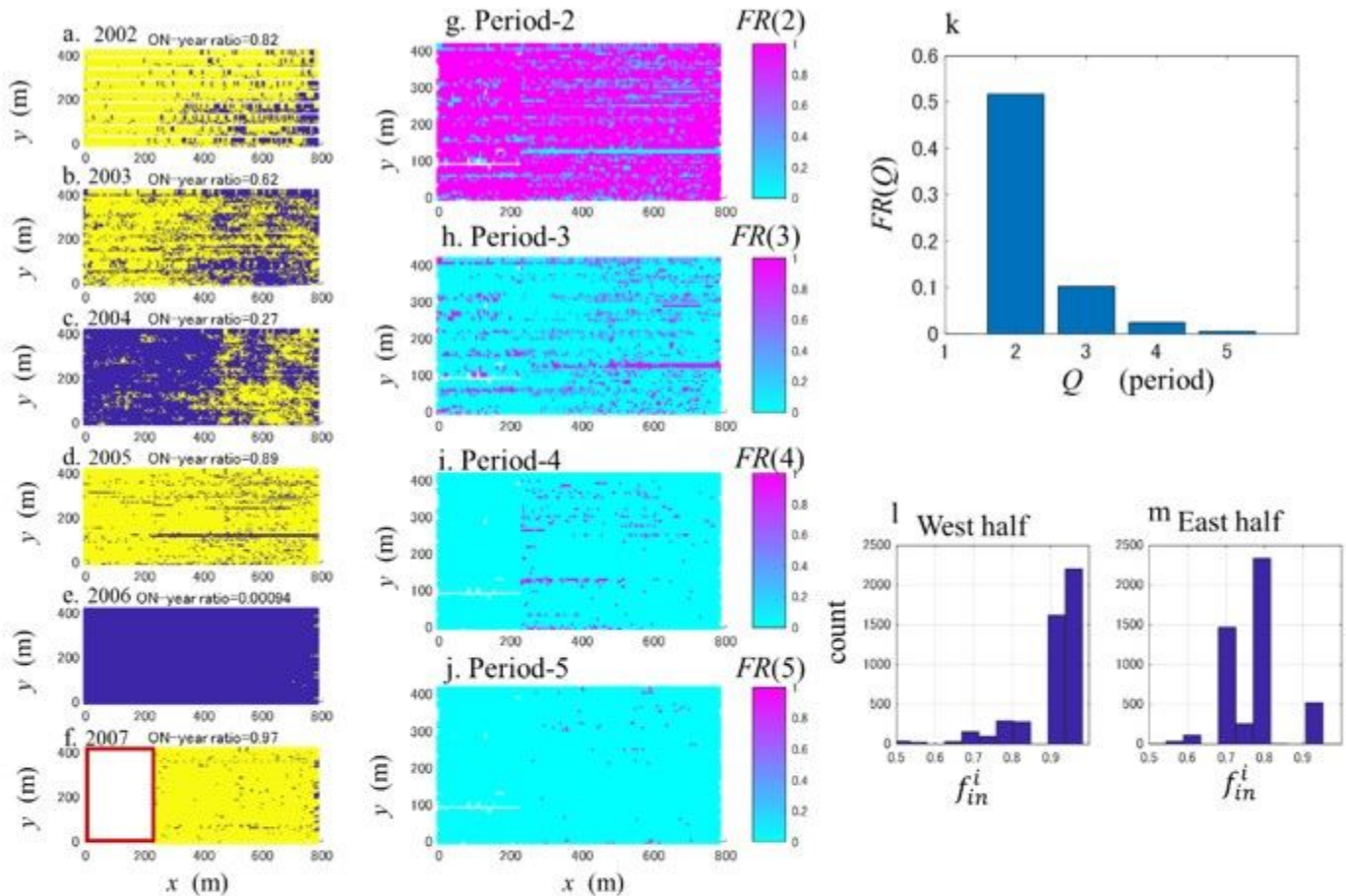


Figure 4 Spatial distribution of the periodic components for individual trees and the compositions of  $FR(Q)$  in the population.

(a)-(f) On-off states of each trees for six years

(g)-(j) Spatial distribution of individual fraction of period  $FR_i(Q)$  for period-two ( $Q=2$ ), period-three( $Q=3$ ), period-four( $Q=4$ ) and period-five ( $Q=5$ ), respectively.

(k) The components of the periodic components  $FR(Q)$  of the population.

(l) Histogram of  $f_{in}^i$  in the west half of the orchard.

(m) Histogram of  $f_{in}^i$  in the east half of the orchard

Figure 4

See image above for figure legend.

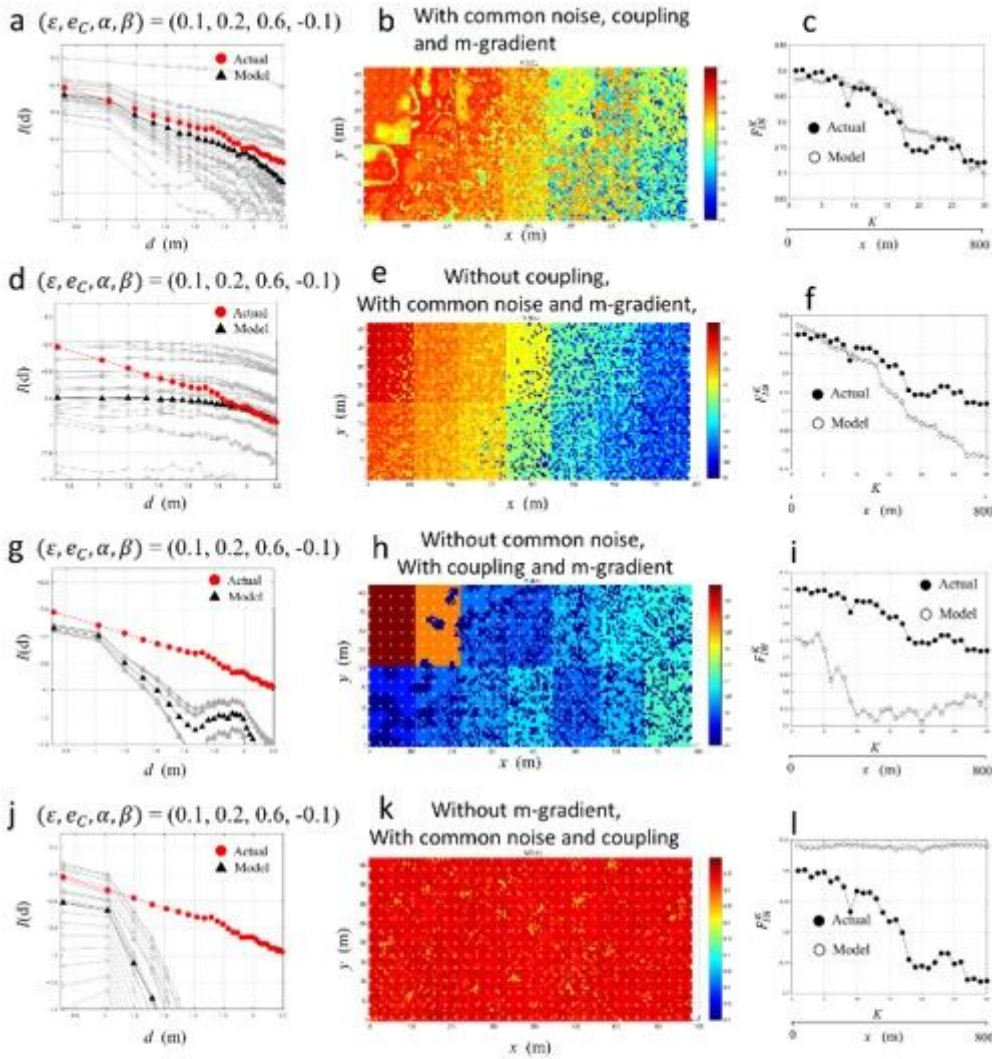


Figure 5. Demonstration of the long-ranged spatial correlations and spatial distribution of phase synchronisation realised by diffusive coupling and common noise in the numerical experiments. The parameter settings used for the numerical simulations are as follows: The first row (a),(b), and (c):with the three essential factors  $(\epsilon, e_C, \alpha, \beta) = (0.1, 0.2, 0.6, -0.1)$ , The second row (d),(e), and (f) : without common noise  $(\epsilon, e_C, \alpha, \beta) = (0, 0.2, 0.6, -0.1)$ , The third row (g),(h), and (i): without the local direct coupling  $(\epsilon, e_C, \alpha, \beta) = (0.1, 0, 0.6, -0.1)$ , The fourth row (j), (k), and (l): without the spatial gradient of cropping coefficients  $(\epsilon, e_C, \alpha, \beta) = (0.1, 0.2, 0, 0)$ , and the fifth row : only with common noise  $(\epsilon, e_C, \alpha, \beta) = (0, 0.2, 0, 0)$ .

## Figure 5

See image above for figure legend.

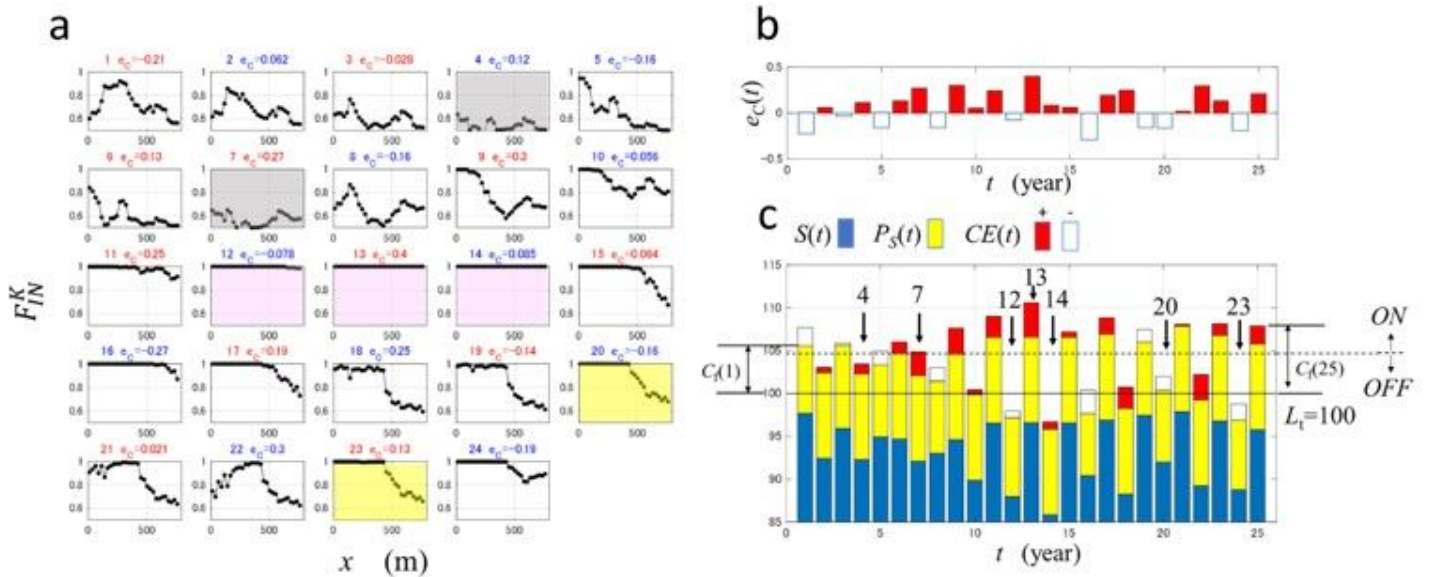


Figure 6. Spatio-temporal behaviour of phase synchronisations caused by endogenous dynamics with exogenous force. The numerical experiments were conducted with the best fit external force (common noise)  $e_c(t)$  and initial values of  $S_i(1)$  ( $i = 1, 2, \dots, 9,562$ ) determined in Fig.5-(b) and calculated 24  $F_{IN}^K(t)$  and  $F_{IN}(t)$ .  $(\varepsilon, e_c, \alpha, \beta) = (0.1, 0.2, 0.6, -0.1)$

(a) 24  $F_{IN}^K(t)$  values are displayed for  $t=1,2,\dots,24$  determined from 25 years runs.

(b) The time (year) history of external force (common noise)  $e_c(t)$ .  $t=1,2,\dots,25$ . “red” and “white” correspond to positive and negative values of  $e_c(t)$ .

(c)  $S(t) = \frac{1}{N} \sum_{i=1}^N S^i(t)$ ,  $N = 9,562$  represents the total amount of resource reserves of all trees at year  $t$ .  $P_S(t)$  is the total resource added on all trees at year  $t$ .  $CE(t) = P_0 \times e_c(t)$  is the external force (common noise) identically imposed on all trees at year  $t$ . In the bar chart, “red” and “white” correspond to positive and negative effects of external forces (common noise);  $CE(t)$ , respectively.

The excess of the threshold ( $L_t=100$ ) of the total amount of  $S(t)$ ,  $P_S(t)$ , and  $CE(t)$  becomes the flowering cost  $C_f(t)$ .

Figure 6

See image above for figure legend.

## Supplementary Files

This is a list of supplementary files associated with this preprint. Click to download.

- [Supplementarydataset.xlsx](#)

- [Supplementsinfo1.docx](#)